1

2

3

4   **Neuron cilia constrain glial regulators to microdomains around distal neurons**

5

6

7   Sneha Ray[1,2], Pralaksha Gurung,[2] R. Sean Manning[1], Alexandra Kravchuk[1,3], Aakanksha

8   Singhvi[1,4],*

9

10

11

12   [1]Division of Basic Sciences, Fred Hutchinson Cancer Research Center, Seattle, WA 98109

13   [2]Neuroscience Graduate Program, University of Washington, Seattle, WA

14   [3]University of Washington School of Medicine, WA 98195

15   [4]Department of Biological Structure, University of Washington School of Medicine, WA 98195

16

17

18

19

20

21   *To whom correspondence should be addressed:

22   Email: asinghvi@fredhutch.org | Tel (206) 667-3606 | Fax (206) 667-5939

23

24 **ABSTRACT**

25 Each glia interacts with multiple neurons, but the fundamental logic of whether it interacts with all

26 equally remains unclear. We find that a single sense-organ glia modulates different contacting

27 neurons distinctly. To do so, it partitions regulatory cues into molecular microdomains at specific

28 neuron contact-sites, at its delimited apical membrane. For one glial cue, K/Cl transporter KCC-3,

29 microdomain-localization occurs through a two-step, neuron-dependent process. First, KCC-3

30 shuttles to glial apical membranes. Second, some contacting neuron cilia repel it, rendering it

31 microdomain-localized around one distal neuron-ending. KCC-3 localization tracks animal aging,

32 and while apical localization is sufficient for contacting neuron function, microdomain-restriction

33 is required for distal neuron properties. Finally, we find the glia regulates its microdomains largely

34 independently. Together, this uncovers that glia modulate cross-modal sensor processing by

35 compartmentalizing regulatory cues into microdomains. Glia across species contact multiple

36 neurons and localize disease-relevant cues like KCC-3. Thus, analogous compartmentalization

37 may broadly drive how glia regulate information processing across neural circuits.

38

39

40

41

42

43

44

45 Key Words: glia, sensory processing, KCC-3, cell polarity, micro-domain

46   **INTRODUCTION**

47   The human brain has about a 100 billion neurons and glia (von Bartheld, Bahney, & Herculano-

48   Houzel, 2016). Glia associate closely with neurons to regulate neuron shape and function, thereby

49   impacting animal behavior (Barres, 2008). Glia do so by molecularly modulating neuron receptive

50   sites (NREs) through extracellular ion buffering, neurotransmitter uptake, cell-signaling, and

51   release of neuroactive substances (Allen & Eroglu, 2017). The observed complexity in both

52   physical and molecular glia-neuron interactions raises a fundamental organizational logic

53   question: does a given glia regulate all contacting neurons/NREs similarly or differently?

54

55   This is relevant because across both central and peripheral nervous systems (CNS and PNS), each

56   glia associates with multiple neurons of different sub-types. In the retina, retinal pigment epithelia

57   glia-like cells contact NREs of rods and different cones, but whether it interacts with them similarly

58   is unclear (Sparrow, Hicks, & Hamel, 2010). In the tongue, Type I glia-like cells contact both Type

59   II and Type III taste cells. Finally, in the CNS, each astrocyte glia can interact with an estimate >

60   1000 neurons, and ~100,000 neuron receptive-endings (NREs), or sites where neurons receive

61   information (Chung, Welsh, Barres, & Stevens, 2015). While it is known that an astrocyte glia

62   regulates excitatory and inhibitory neurons differently (Eroglu et al., 2009; Stogsdill et al., 2017),

63   whether or how cellular specificity dictates glia-neuron interactions at individual NREs remains

64   largely unexplored at molecular detail.

65

66   The cellular and molecular asymmetry within both CNS and PNS glia hints that these cells can

67   have non-uniform interactions with contacting cells. For one, glia in both settings exhibit

68   signatures of polarity, with apical and basolateral proteins segregating into discrete glial

69   membranes. For example, in PNS Schwann cells, apical membranes contact axons and basolateral

70   regions face the extracellular matrix (Belin, Zuloaga, & Poitelon, 2017). Similarly, for RPE glia-

71   like cells in the retina, basolateral proteins, such as the bestrophin chloride channel, abut the

72   vascular choroid, while apical proteins, such as the Na+/K+-ATPase, face the photoreceptors

73   (Gallemore, Hughes, & Miller, 1997; Strauss, 2005). CNS glia also have striking finer-grained

74   molecular asymmetry, and localize specific molecules not only by apical-basal polarity, but into

75   even more discrete sub-compartments, or microdomains. Thus, CNS astrocytes enrich basolateral

76   markers such as AQP4/Aquaporins at their end-feet around epi/endothelia, Ezrin and mGluR3/5

77   at perisynaptic astrocytic processes, and GLT-1 and other transporters at synapses (Murphy-royal

78   et al 2015). Drosophila ensheathing glia contain basolateral membranes, enriched with PIP3 and

79   the Na+/K+-ATPase Nervana2, that face the extracellular matrix and an apical membrane, rich

80   with PIP2 and sub-membranous β_H-spectrin, that face the neuropil (Pogodalla et al., 2021). Finally,

81   CNS astrocytes have not only molecular, but also functional microdomains, wherein they exhibit

82   different intracellular Ca2+ dynamics to different circuit activities (Khakh & Sofroniew, 2015).

83   This suggests that glia differentiate inputs across contacting neurons.

84

85   *C. elegans* presents a powerful and genetically tractable experimental model to investigate

86   specificity in glia-neuron interactions, at single-cell resolution (Oikonomou & Shaham, 2011;

87   Singhvi & Shaham, 2019; Singhvi, Shaham, & Rapti, 2023). The animal's nervous system

88   comprises 56 glia and 300 neurons, each of which makes stereotypic and invariant glia:neuron

89   contacts (Oikonomou & Shaham, 2011; Singhvi & Shaham, 2019; Singhvi et al., 2023).

90   Furthermore, prior work has demonstrated that *C. elegans* glia regulate their associate NRE shape

91   and function, with consequences on sensory behavior (Martin, Bent, & Singhvi, 2022; Raiders et

92   al., 2021; Singhvi et al., 2016; Wallace et al., 2016). They also exhibit functional Ca^{2+} dynamics

93   to a subset of neuron functions (Ding et al., 2015; Duan et al., 2020). Finally, it has been shown

94   that loss of individual glia has varying impact on different associated neuron properties (Bacaj,

95   Tevlin, Lu, & Shaham, 2009).

96

97   To examine specificity in glia-neuron interactions, we focused on one *C. elegans* glia cell, the

98   amphid sheath (AMsh) glia. It is one of two glial cells in the animal's major sense organ called the

99   amphid, at the anterior nose-tip (Singhvi & Shaham, 2019). The AMsh glia interacts with NREs

100   of 12 different sensory neurons, each of which senses a distinct sensory modality (Figure 1A)

101   (Singhvi & Shaham, 2019). Thus, impact of AMsh glia on individual NREs and animal sensory

102   behaviors can be examined reproducibly in vivo at single-cell resolution. Of the 12 neurons, AMsh

103   glia create an autotypic channel around 8 of the NREs (Perens & Shaham, 2005; Perkins,

104   Hedgecock, Thomson, & Culotti, 1986). Prior work has identified molecular pathways that

105   regulate the size of the channel lumen through DAF-6/Patched and LIT-1/Nemo kinase pathways

106   (Oikonomou et al., 2011; Perens & Shaham, 2005). Independently, we and others previously

107   showed that AMsh glia uses the potassium chloride cotransporter KCC-3 to regulate the NRE

108   shape and function of the animals major thermosensory neuron, the AFD, and consequently,

109   animal thermosensory behaviors (Singhvi et al., 2016; Yoshida et al., 2016).

110

111   Here, we report that AMsh glia compartmentalizes interactions with different NREs, with KCC-3

112   specifically regulating the shape of only the AFD-NRE. First, we find that KCC-3 localizes to an

113   apical microdomain in glia. Our investigation into the molecular basis of this glia-neuron contact

114   specificity revealed that KCC-3 localizes to a micro-domain within the glial apical membrane

115   apposing only AFD-NRE contact sites and excluded from other NRE contact sites. Our studies

116   find that both cell-intrinsic and non-autonomous mechanisms cooperatively drive KCC-3's

117   polarized apical and microdomain localization through distinct protein domains. Surprisingly,

118   rather than AFD-NRE recruiting it, we find that cilia of heterotypic amphid NREs repel KCC-3,

119   leading to its restrained apical micro-domain localization around AFD-NRE. Specifically, we

120   identify the contacting ciliated NREs of two other AMsh-glia associated neurons (AWC and ASE),

121   as sufficient to localize KCC-3 into a micro-domain. Finally, we show that this exquisitely

122   regulated KCC-3 localization is required for its regulation of AFD-NRE shape and functions.

123   Unexpectedly, our studies also reveal a role for KCC-3 in regulating other amphid neuron

124   functions, including AWC, as well as interactions between the different glial regulatory cues.

125   Taken together, these results provide molecular insight into how specificity in glia-neuron

126   interaction is driven by compartmentalization of individual glial regulatory cues, and regulation of

127   which impacts cross-modal sensory processing.

128

129   **RESULTS**

130   **AMsh glial K/Cl transporter localizes to a micro-domain around the AFD neuron**

131   We previously uncovered that the cation-chloride cotransporter KCC-3 acts in AMsh glia to

132   regulate AFD-NRE shape and associated animal behavior (Singhvi et al., 2016). Intriguingly, we

133   noted that a translational KCC-3:GFP reporter strain did not localize uniformly throughout the

134   AMsh glial membrane (Figure S1A). To verify this, we engineered a dual-labeled transgenic strain

135   with AMsh glia labeled by cytosolic CFP and KCC-3 tagged with mScarlet, and again found its

136   localization was biased anteriorly, where the glia physically contacts 12 associated NREs,

137   including AFD-NRE (Figure 1A-B'').

138

139   In both confocal and 3D-SIM super-resolution microscopy, we further observed sub-cellular

140   enrichment of KCC-3:mScarlet to a micro-domain in anterior glial membranes (Figure 1C-C'').

141   The pattern of KCC-3:mScarlet enrichment was anatomically reminiscent of AFD-NRE microvilli

142   shape (Figure 1C'). We therefore performed double transgenic labeling of KCC-3 with reporters

143   marking each of the different classes of AMsh glia-associated NREs (villi:AFD,

144   wing:AWA/AWB/AWC, channel:ASE) (Figure 1D-I'', S1B-B''). This revealed that KCC-

145   3:mScarlet predominantly localizes to glial membrane contact site only around AFD-NRE and is

146   excluded from glial contact sites around other NREs. This localization indicates that KCC-3 is a

147   facile molecular tool to interrogate how glia specifically target cues to subsets of contacting

148   neurons.

149

150   **KCC-3 localizes to an apical micro-domain in AMsh**

151   In addition to its micro-domain localization adjacent to only AFD NREs, KCC-3:mScarlet also

152   has an anterior "tail" that extends ~50um from the animal nose tip (Figure 1B'). This tail was

153   reminiscent of the observed expression of apical markers in glia (Low et al., 2019; Martin et al.,

154   2022). To examine this closely, we first adapted previously reported SAX-7/L1CAM based

155   polarity markers under the AMsh glia-specific $P_{F53F4.13}$ promoter. As expected, we found that glial

156   basolateral domains appose epithelia laterally and label the entire glial cell, including its cell body

157   and process (Figure S2A). Apical membranes, on the other hand, are restricted to the anterior

158   region of the cell, where the glia contacts NREs, and terminate in a discrete "tail" at the anterior

159   head of the animal (Figure S2B), called hereafter the "glial apical boundary", or GAB.

160   Simultaneous co-labeling of both apical and basolateral domains in animals indicates that apical

161   membranes appose neuron-contact sites while basolateral domains face outward lumen (Figure

162   2A-D). This localization pattern led us to posit that KCC-3 is constrained to an apical microdomain

163   in glia.

164

165   Since it is formally possible that SAX-7 based markers inadvertently alter cell:cell adhesion, we

166   first chose to confirm glial apical domain identity independently. We expressed a PH-PLCδ:GFP

167   apical membrane marker (Mahon, 2011) under an AMsh glia-specific promoter, and found that it

168   labels the apical membrane and GAB, similar to SAX-7-based constructs (Figure S2C). Thus, this

169   expression pattern reflects glial apical domain and is not an artefact of aberrant SAX-7 adhesion.

170

171   Next, we overlaid apical and basolateral membrane reporters with markers for AMsh-glia

172   specific KCC-3:mScarlet. We found that the apical AMsh marker and KCC-3 colocalize at the

173   anterior glial ending, including at the GAB, confirming that KCC-3 localizes to glial apical

174   membranes (Fig. 2E-FG''). Of note, however, KCC-3 expression was restricted to a sub-set of the

175   apical membrane labeling, consistent with it being excluded from non-AFD contact sites (Fig. 2F-

176   F'', hash). We did not observe any KCC-3:mScarlet overlay with the basolateral AMsh membrane

177   marker (Fig. 2H-H''). These results show that in AMsh glia, KCC-3 localization is restricted to an

178   "apical micro-domain" specifically at the glia's AFD-NRE contact site.

179

180   It has been proposed that glia are analogous to neuroepithelia (Low et al., 2019). Apical-basal

181   domains in epithelia are delimited by tight junction (Shin, Fogg, & Margolis, 2006). We therefore

182   asked if GAB was contained by junctional proteins. However, we found that while the tight-

183   junction marker AJM-1 localizes around the glia:NRE contact site, it does not bound the GAB

184   domain marked by either KCC-3 or apical markers (Figure 2H-H''). To confirm this striking result,

185   we also examined KCC-3 expression pattern with DLG-1/DiscsLarge, another junctional marker

186   (McMahon, Legouis, Vonesch, & Labouesse, 2001), and found again that the GAB was not

187   delimited by DLG-1 (Figure S2D-D''). Thus, AMsh glial KCC-3 localization to an apical

188   microdomain is distinct from tight junction-delimited epithelia-like polarity.

189

190   We previously identified that mutations in UNC-23/BAG2 induce expansion of glial apical

191   membranes (Martin et al., 2022). We found that loss of *unc-23* caused expansion of KCC-3

192   microdomains, tracking behavior of other apical markers in *unc-23* mutant animals (Figure S2E).

193   This corroborated that KCC-3 is an apical membrane protein, and is regulated like other AMsh

194   apical proteins at the GAB.

195

196   Finally, AFD-NRE shape deteriorates with animal age and *kcc-3* mutants exhibit age-dependent

197   defects in AFD-NRE shape (Huang et al., 2020) We therefore wondered if KCC-3 localization

198   tracks AFD-NRE aging. We performed longitudinal examination of KCC-3 sub-cellular

199   localization in AMsh glia. When expressed under the heterologous AMsh-glial specific $P_{F53F4.13}$

200   promoter, we observed that KCC-3 apical micro-domain in developing L2 larva that is maintained

201   into adulthood (Figure 2I-K). As $P_{F53F4.13}$ does not express embryonically, we determined when

202   KCC-3 localization initates by examining rare mosaic transgenic animals with KCC-3:GFP driven

203   under its own promoter. We found that KCC-3 expresses and localizes shortly after AMsh glia are

204   born in the embryo (Figure S2F-G). Strikingly, the microdomain localization, but not GAB

205   boundary, lost fidelity with age (Figure 2L-M), correlated with age-dependent decline in AFD-

206   NRE shape (Huang et al., 2020).

207

Glial KCC-3 localization is independent of AFD neuron shape or function

209   Given KCC-3 localization specifically around AFD-NRE, a parsimonious model would be that

210   AFD-NRE recruits glial KCC-3 localization. Since the AFD-NRE is the primary thermosensory

211   apparatus in the animal (Goodman & Sengupta, 2018; Kimura, Miyawaki, Matsumoto, & Mori,

212   2004), we first wondered if temperature regulates recruitment of glial KCC-3 to AFD-NRE contact

213   site. However, we found that animals maintained KCC-3 apical microdomain localization,

214   irrespective of their cultivation temperature (Figure S3A). Consistent with this, we also found that

215   animals mutant for the sole CNG channel β-subunit required for AFD activity, TAX-2, also show

216   intact KCC-3 localization (Coburn & Bargmann, 1996) (Figure 3A). Furthermore, KCC-3 still

217   localizes to an apical micro-domain in *ttx-1* mutants which lack AFD-NRE microvilli that house

218   the neuron's sensory apparatus (Figure 3A) (Satterlee et al., 2001). Finally, the receptor guanylyl

219   cyclase GCY-8 regulates AFD thermosensory transduction through cGMP signaling with GCY-

220   18 and -23 (Inada et al., 2006). We previously showed that GCY-8 is inhibited directly by KCC-

221   3-dependent chloride, and *gcy-8(ns335)* have constitutively activated cGMP production with

222   consequently truncated AFD-NRE (Singhvi et al., 2016). Animals with a gain-of-function *gcy-*

223   *8(ns335)* mutation, show intact KCC-3 localization (Figure 3A). Together, these results show that

224   AFD-NRE shape or function do not drive KCC-3 localization.

225

226   To test if AFD neuron altogether is dispensable, or if it has other properties driving KCC-3

227   localization, we next ablated the neuron altogether, in two temporally distinct ways (Figure 3B).

228   First, we expressed the pro-apoptotic factor EGL-1 under an AFD specific-promoter (P_{srtx-1}) to

229   ablate AFD genetically (Nehme & Conradt, 2009; Singhvi et al., 2016) . We first confirmed that

230   the P$_{srtx-1}$ promoter is expressed starting shortly after AFD's birth in the 3-fold stage embryo,

231   indicating that it should ablate the neuron embryonically (Figure S3B-B''). Second, we used laser

232   microsurgery to ablate the AFD nuclei in L1 larvae (Sulston, 1983). In either case, successful AFD

233   ablation was tracked by complete disappearance of P$_{srtx-1}$:GFP (Figure S3D). Surprisingly, we

234   found that glial KCC-3 maintained restricted location to an apical microdomain in in both

235   scenarios (Figure 3C, S3C). Taken together, our results show that while glial KCC-3 localizes to

236   AFD-NRE contact sites, the AFD neuron or its sensory cue, NRE shape, or activity are not required

237   for glial KCC-3 glial microdomain localization.

238

239   **Cilia of distal glia-associated neurons restrain glial KCC-3 to AFD-NRE**

240   If AFD neuron/NRE does not recruit glial KCC-3, we hypothesized two, mutually non-exclusive,

241   models of glial KCC-3 localization: (i) it is repelled by other NREs or (ii) its localization is

242   regulated cell-autonomously by glia.

243

244   To test a role for other NREs, we noted that these are all derived cilia (Figure 3D). We therefore

245   examined KCC-3 localization in animals mutant for the ciliary DAF-19/RFX transcription factor

246   regulating all ciliary factors, and which have a complete loss of all cilia (Fig. 3E-F'') (Perkins et

247   al., 1986; Swoboda, Adler, & Thomas, 2000). We found that *daf-19* mutants had defects in

248   microdomain localization, but not apical enrichment of KCC-3. Specifically, in these mutants,

249   KCC-3 is still enriched apically, with the characteristic tail, but is no longer excluded from non-

250   AFD-NRE contacting glial membranes (Fig. 3F-F'').

251

252   Both ciliogenesis and transport of ciliary proteins are mediated by intraflagellar transport (IFT)

253   bidirectionally along ciliary microtubules (Lechtreck, 2015). Briefly, IFT transport is mediated by

254   the multi-protein subcomplexes A and B, and aided by BBS regulatory proteins, to bind cargo.

255   Transport along microtubule tracks is guided anterogradely by Kinesin II (heterotrimer) and OSM-

256   3 (homodimer) and retrogradely by Dynein motors. Shuttling from cell-body to cilia is guided by

257   the clathrin coated vesicle adaptor protein-1 (AP-1) (Dwyer, Adler, Crump, L'Etoile, & Bargmann,

258   2001) (Figure S3E). To confirm the requirement for intact ciliary transport in glial KCC-3

259   localization, we performed a candidate screen of all these components. We found that loss of any

260   of these ciliary components, including OSM-3/kinesin, CHE-11/IFT-A component, DYF-11/IFT-

261   B component, OSM-6/IFT-B component, BBS-8/BBsome or UNC-101/AP1, led to aberrant

262   expansion of glial KCC-3 apical microdomain localization to non-AFD-NRE contact regions

263   (Figure 3E). Of note, except for UNC-101/AP1, enrichment around AFD-NRE was maintained

264   (Figure S3F).

265

266   Finally, a simple caveat to these interpretations might be that the KCC-3 localization appears

267   aberrant in cilia mutants as a secondary consequence of altered AMsh glia anterior ending shape.

268   We therefore examined AMsh morphology in *daf-19* and *dyf-11* mutant animals. Tracking prior

269   EM evidence (Bacaj, Lu, & Shaham, 2008; Perens & Shaham, 2005; Perkins et al., 1986)we found

270   that AMsh glia anterior ending shape was grossly normal in both mutants, albeit marginally

271   shrunken in *daf-19* mutant animals (Figure SG-I). Taken together, we infer that a transported

272   ciliary protein in non-AFD NREs guides KCC-3 localization by repulsion from non-AFD-NRE

273   contact sites, rather than recruitment to AFD-NRE.

274

275   **A two-neuron ciliary signal drives glial KCC-3 localization**

276   We next decided to identify the neurons whose ciliary NREs regulate KCC-3. First, we examined

277   a mutation in OIG-8/Ig domain protein, known to regulate ciliary elaboration of embedded "wing"

278   neurons (Howell & Hobert, 2017) as well as a mutation in the CHE-12/HEAT domain protein,

279   which only impacts "channel" neurons (Bacaj et al., 2008). *oig-8* mutants exhibit partial defects,

280   similar to, but not phenocopying cilia mutant defects, while *che-12* mutants had no effect on KCC-

281   3 localization (Figure 3E). A parsimonious interpretation of this data is that KCC-3 localization is

282   driven primarily by one or more wing neurons, with channel neurons playing a lesser role. We

283   tested this hypothesis through both candidate and unbiased cell-biology screening approaches.

284

285   First, in the candidate approach, we asked if cellular subtype identities of wing neurons are

286   relevant. For this, we examined animals bearing mutations in ODR-7/NHR (AWA identity), CEH-

287   37/Otx homeodomain (AWB identity), CEH-36/Otx (AWC identity) and CHE-1/GLASS Zn

288   finger (ASE identity) (Lanjuin, VanHoven, Bargmann, Thompson, & Sengupta, 2003; Sengupta,

289   Colbert, & Bargmann, 1994; Uchida, Nakano, Koga, & Ohshima, 2003). These genes act in

290   parallel to DAF-19 to elaborate specific NRE cilia shapes (Figure S3J) (Lanjuin & Sengupta 2004).

291   In these mutants, ciliary structures are altered or mis-specified into that of another "wing" neuron

292   but are not missing. Curiously, none of these mutants perturbed KCC-3 localization (Figure 3G),

293   suggesting that cellular identity of any of these four individual neurons is not sufficient to drive

294   KCC-3 restricted localization. To validate this in an orthogonal approach, we also performed laser

295   ablation of all wing neurons (AWA/B/C) individually and found that this did not alter KCC-3

296   localization (Figure 3G). Thus, individual wing neurons, or channel neurons alone, are not

297   sufficient to guide KCC-3 restriction, implying that a redundant subset of neurons is required.

298

299   To identify this combination, we turned to an unbiased cell-specific rescue approach, wherein we

300   probed which neuron expression of DYF-11 is sufficient in to rescue KCC-3 localization defect of

301   *dyf-11* mutant animals (Fig. 3H-I). For this, we first established the validity of our approach by

302   confirming that KCC-3 localization is rescued by DYF-11 expressed under its native P_{dyf-11}

303   promoter (Figure 3H-I). Similarly, DYF-11 expression under P_{gpa-3} and P_{tax-4} promoters, which

304   express in 9 and 10 amphid neurons, respectively, rescues KCC-3 localization (Figure 3H-I). We

305   next tested differing subset of amphid neurons by the non-overlapping $P_{R102.2}$ or (P_{flp-19} + P_{odr-1})

306   combination promoters to guide DYF-11 rescuing construct in channel neurons or all wing

307   neurons. Interestingly, both promoters rescued equally, revealing that either combination of

308   amphid ciliary NREs can guide KCC-3. Finally, P_{ceh-36}, which expresses in AWC+ASE, and P_{odr-1},

309   which expresses in AWC+ AWB neurons, both rescued the phenotypic defects. This identifies

310   AWC+X as a minimal neuron combination that guides KCC-3 localization. As such, expression

311   under P_{odr-4} (2 channel neurons) and $P_{SRTX-1B}$ (AFD) was insufficient to rescue KCC-3 localization.

312   These results also explain why single-neuron ablation or terminal cell-fate specification did not

313   impact KCC-3 localization, and reveal that, minimally, AWC neurons acts with a second neuron

314   (can redundantly be either wing or channel) to guide glial KCC-3 microdomain localization around

315   AFD-NRE.

316

317   **Glial KCC-3 microdomain does not require canonical KCC regulators**

318   The NRE ciliary signal needs to be received and transmitted to KCC-3 to maintain its localization.

319   WNK and the GCK Ste20 kinases SPAK/PASK and OSR, regulate cation chloride transporters

320   like KCC-3 across systems and species (Alessi et al., 2014; Blaesse, Airaksinen, Rivera, & Kaila,

321   2009; Hisamoto et al., 2008; Kaila, Price, Payne, Puskarjov, & Voipio, 2014; Payne, Rivera,

322   Voipio, & Kaila, 2003). We therefore first asked if they are involved in this process. The *C. elegans*

323   genome encodes a single WNK ortholog (WNK-1) (Hisamoto et al., 2008). We assessed KCC-3

324   localization in both a loss of function WNK-1 mutation and via RNAi and found that neither

325   regulates AMsh glial KCC-3 localization (Figure S4A-B). Consistent with this, alignment of *C.*

326   *elegans* KCC-3 with mammalian orthologs did not identify the conserved WNK and GCK kinase

327   motif or phosphorylation sites (Figure S4C-E). We also examined mutations in the ARGK-

328   1/creatine kinase, which localizes with KCC-3 (Burgess, Shah, Hough, & Hynynen, 2016; Salin-

329   Cantegrel et al., 2011), and found no effect on KCC-3 localization (Fig. S4A). Finally, we have

330   previously identified a role for the apical cytoskeletal SMA-1/β_H-Spectrin in AMsh apical polarity

331   regulation (Martin et al., 2022). However, animals with genetic lesions in *sma-1* exhibited normal

332   KCC-3 localization (Figure S4A). Thus, localization of glial KCC-3 membrane transporter to

333   apical membranes is independent of the apical SMA-1/β_H-Spectrin cytoskeleton. Together, these

334   results indicate that AMsh glia restricts KCC-3 localization to an apical microdomain independent

335   of previously identified kinase regulators of cation-chloride transporters.

336

337   **A two-step model for KCC-3 apical microdomain localization**

338   To understand how KCC-3 is localized, we decided to define the minimal KCC-3 sequences

339   required for localization. First, we expressed *C. elegans* K/Cl homologs fluorescently tagged KCC-

340   1 or KCC-2 under the AMsh glial promoter to ask if these sequentially similar proteins localize to

341   an apical micro-domain like KCC-3 (Figure 4A). Both proteins in fact localized to AMsh glial

342   basolateral membranes, in striking contrast to KCC-3 (Figure 4B-E). This indicates that sequences

343   dissimilar between KCC-1/KCC-2 and KCC-3 drive KCC-3's apical and micro-domain

344   localization. Our *in silico* sequence alignment suggested that the sequence dissimilarity between

345   KCC-2 and KCC-3 was largely restricted to three protein domains: the N-terminal, the large

346   extracellular loop (LEL) between TM5 and TM6, and a short 81 amino acid region of the C-

347   terminal (Figure 4F). To identify if any of these regions were relevant, we created chimera KCC

348   proteins within each and examined localization of the chimera within AMsh glia to either a

349   microdomain, apically, basolaterally, or elsewhere (Figure 4G-I, S6A-B).

350

351   First, we swapped the predicted N-terminal 90 AA sequence of KCC-3 with the 84 AA equivalent

352   aligned sequence of KCC-2 (Figure S5A). This was sufficient to drive the chimera basolaterally

353   (Figure 4J), suggesting that sequences contained within drive basolateral targeting of KCC-2. To

354   narrow this further, we further swapped the first 55 amino-acid sequence of KCC-3 with the 41

355   amino-acid equivalent aligned sequence of KCC-2. This too drove the chimera basolaterally

356   (Figure 4J). We divided this region further by generating a KCC-3 chimera with the first 20AA as

357   KCC-2, but this failed to target the protein basolaterally, suggesting that the basolateral targeting

358   sequence resides between 21-41AA in KCC-2 (Figure S6C-D). We were unable to identify a

359   shorter basolateral targeting sequence within this 19AA KCC-2 N-terminal region by either site-

360   directed mutagenesis of predicted phosphorylation and dileucine sites, or shorter sequence

361   deletions (Fig. S4C-D). We also tested and found that KCC-3 N-terminal sequence is not sufficient

362   to traffic KCC-2 protein apically (Figure 4J). Indeed, we note punctate staining in internal

363   vesicular compartments, suggesting that lack of basolateral targeting motifs likely stall KCC-2

364   membrane targeting. Finally, for completeness, we also tested if it was possible that a region in

365   KCC-3's equivalent 55AA N-terminal sequence blocks a basolateral targeting motif. Again, we

366   curated site-directed mutagenesis or shorter deletions in KCC-3 were unable to drive it

367   basolaterally, suggesting this is likely not the case (Figure S6C-D). We conclude that a large and/or

368 redundant sequence motif within a 19AA N-terminal sequence (AA21-41) drives KCC-2

369 basolaterally, and lack of this motif allows other domains to traffic KCC-3 apically.

370

371 To identify micro-domain motifs in KCC-3, we next engineered additional chimera proteins with

372 varying KCC-2 C-terminal sequence. A chimera with KCC-3 sequence until the C-terminal region

373 of high sequence dissimilarity (C-term swap A), with the last 155 AA of KCC-3 swapped with the

374 equivalent 171 AA of KCC-2, localizes apically (Figure 4J, S5B). A chimera that with KCC-3

375 until just after the C-terminal region of high sequence dissimilarity (C-term swap B), with the last

376 68 AA of KCC-3 swapped with the equivalent 66 AA of KCC-2, exhibited faithful KCC-3

377 localization (Figure 4J, S5B). We therefore infer that the major microdomain-targeting motif

378 resides in a region of high sequence dissimilarity between KCC-3 and KCC-1/2, amid amino acids

379 915-997 of KCC-3 (Figure S5B). However, while necessary, we note that these sequences are not

380 sufficient to override the strong basolateral targeting sequences of KCC-2 (Figure 4J), but only

381 operate when this basolateral motif is absent.

382

383 Since K/Cl proteins exist as oligomers (Simard et al., 2007) and the dimerization domain is thought

384 to reside in the cytosolic C terminus, it is possible that dimerization would impact our inference of

385 the motifs above. We asked if microdomain localization of the chimera was due to its shuttling

386 with endogenous protein as a heterodimer. To test this, we examined localization of these chimeras

387 in *kcc-3(ok228)* mutant animals. We found that trends hold equally in both wild type and mutant

388 background (Figure S6E). Indeed, our results support the notion that if at all, endogenous protein

389 may even partly hinder chimera localization. Thus, cross-oligomerization with wild-type protein

390 cannot explain the ability of C-terminal chimeras to localize to a microdomain.

391

392   Together, these results reveal a two-step model for glial KCC-3 localization. First, lack of

393   basolateral-targeting motifs in KCC-3 N-terminal region allows it to be shuttled apically to GAB.

394   Once there, ciliary NRE signals act with the C-terminal 915-997 AA sequence to restrict KCC-3

395   to a microdomain.

396

397   **AMsh glial KCC-3 micro-domain localization regulates AFD neuron shape and function**

398   Having investigated how, we next asked why AMsh glia and non-AFD NREs regulate KCC-3

399   localization. We hypothesized that it could play two roles; (a) regulation of AFD-NRE function,

400   and (b) prevent it from aberrantly impacting other NRE functions. To test this, we examined

401   properties of both AFD and other NREs, in *kcc-3(ok228)* mutant and mis-localized KCC-3

402   transgenic animals.

403

404   First, we asked if KCC-3 localization impacted AFD-NRE shape. Exploiting the fact that *kcc-3*

405   mutants have disrupted AFD-NRE shape (Figure 5A-A') (Singhvi et al., 2016), we examined if

406   mis-localized KCC-3 chimeras can rescue AFD shape in a *kcc-3* mutant background. While

407   expression of full-length KCC-3 in a *kcc-3* background rescues AFD shape, a basolaterally

408   localized chimera (KCC-2^{Nterm} in an otherwise KCC-3 protein) fails to rescue AFD shape (Fig.

409   5B). In contrast, a chimera that shows apical localization was able to rescue *kcc-3(ok229)* mutant

410   AFD-NRE defects (Figure 5B), even if slightly less efficiently than a microdomain-exclusive

411   construct. Together, we infer that apical localization, but not necessarily micro-domain

412   localization, KCC-3 is required for its regulation of AFD-NRE shape.

413

414 We also asked the corollary—is aberrant apical expansion of KCC-3 detrimental to AFD-NRE

415 shape? *dyf-11* and *osm-6* mutant animals, where AMsh glial KCC-3 enriches around AFD-NRE

416 besides also expanding aberrantly to other NREs (Figure 3E), do not exhibit defects in AFD-NRE

417 shape (Singhvi et al 2016). Thus, we conclude that enrichment of KCC-3 regulates AFD-NRE

418 shape but its expansion to other apical regions is inconsequential to the AFD.

419

420 **AMsh glial KCC-3 regulates distal AWC neuron activity**

421 If KCC-3 expansion is inconsequential to AFD-NRE, why is it regulated? We decided to formally

422 test if KCC-3 can impact other NRE properties, despite not localizing to their membrane contact

423 sites (Figure 1G-I'', S1B-B''). As expected, we found that loss of *kcc-3* does not impact the shape

424 of the wing neurons (AWA, AWB, AWC), and the channel neuron ASE (Figure 5C-F', S7A).

425 Surprisingly, however, *kcc-3(ok228)* null mutant animals exhibited behavioral defects in *kcc-3*

426 mutants for wing neuron-driven animal behaviors. Specifically, *kcc-3* mutant animals fail to

427 chemotax towards the AWA-sensed odorants methyl pyrazine and diacetyl and the AWC-sensed

428 odorants isoamyl alcohol and benzaldehyde (Figure 5G-I). These deficits were comparable to

429 defects in AMsh glia-ablated animals and previously reported behavior loss of DYF-11/IFTB

430 (Figure S7B-C) (Bacaj et al., 2008, 2009). Animal behavior mediated by the ASE-channel neuron

431 sensed tastant 10mM NaCl is, however, unaffected (Figure 5J).

432

433 We asked if these defects were secondary to *kcc-3(ok228)* AFD-NRE defects through indirect

434 electrical or chemical synaptic deficits between AFD and other neurons. To parse this, we tested

435 *ttx-1* mutants, which lack AFD-NRE for these behaviors and observed normal chemotaxis

436 behaviors towards methyl pyrazine, isoamyl alcohol, and benzaldehyde (Figure S7B). Thus,

437   defects in AFD-NRE shape or functions alone cannot explain the observed deficits in AWA/C

438   functions.

439

440   Next, we wondered if the defects arose from KCC-3 requirement in AMsh glia, or its indirect

441   function in other glia that associate with the downstream circuit interneurons (Singhvi & Shaham,

442   2019; White, Southgate, Thomson, & Brenner, 2008). To test this, we asked if expression of KCC-

443   3 only in AMsh glia could rescue the AWA/C wing-neuron behavior defects. We found that it

444   could for AWC-dependent behaviors but only partially rescues AWA- or AWB- dependent

445   sensory animal behaviors (Figure 5H-I). We infer that AMsh glial KCC-3 can indirectly affect

446   AWC function, despite not localizing to the glial contact site of this neuron/NRE. Defects in AWA-

447   dependent behaviors may arise from a combined requirement of KCC-3 in AMsh and other glia.

448

449   We therefore decided to focus on AWC, and examine how its neuron activity profiles track KCC-

450   3 by functional imaging of intracellular Ca^{2+} dynamics using a cell-specific expression of

451   fluorescent reporter GCaMP (Chalasani et al., 2007). Tracking animal behavior data, we observed

452   attenuated reponses of the AWC neuron to iso-amyl alcohol (Figure 6A, 6C, 6D). More

453   interestingly, when challenged with the odor a second time with a 30s interval, the attenuation in

454   AWC responses was larger (Figure 6B). Thus, while not present at its contact-sites, glial KCC-3

455   can nonetheless regulate neuron response properties of the distal AWC-NRE.

456

457   **All glial microdomains do not impact distal neurons**

458   KCC-3 regulates AWC-dependent sensory animal behaviors, leading us to wonder if all

459   microdomains can distally regulate other neuron functions. The identity of the AWC molecular

460   microdomain, if any, is unknown, so we asked if channel microdomain cues regulate AFD-NRE.

461   We found that *daf-6* and *vap-1* lesions do not exhibit significant defects in AFD-NRE shape

462   (Figure S7D) and *daf-6* or *che-14* do not impair AFD-mediated thermotaxis behaviors (Perkins et

463   al., 1986). *daf-6* and *che-14* also do not impact sensory behaviors to volatile odorants mediated by

464   wing-neurons (Albert, Brown, & Riddle, 1981; Bargmann, Hartwieg, & Horvitz, 1993). Thus,

465   unlike KCC-3, channel microdomain cues do not modulate distal NREs, suggesting specificity

466   with which these are regulated.

467

468   **AMsh glia's multiple apical microdomains are regulated independently**

469   The results above show that compartmentalized localization of specifically KCC-3 drives cross-

470   modal sensory processing of both AFD-dependent thermotaxis and AWC-dependent chemotaxis

471   behaviors. How is this coordinated within a glial cell? We tested the hypothesis that KCC-3 may

472   do so by altering other glial microdomains.

473

474   Previously, it has been shown that the AMsh glia localizes the secreted molecule VAP-1 and

475   membrane-associated LIT-1/NEMO-like kinase at the channel (Oikonomou et al., 2011; Perens &

476   Shaham, 2005). We find that KCC-3 localizes around AFD-NRE. Together, this implies that AMsh

477   glia make at least three molecular microdomains – around channel NREs (VAP-1/LIT-1 positive,

478   KCC-3 negative), AFD-NRE (VAP-1/LIT-1 negative, KCC-3 positive), and wing neurons (VAP-

479   1/LIT-1 negative, KCC-3 negative). To confirm this, we engineered transgenic animals that

480   simultaneously labeled these glial cues and found that KCC-3 indeed localizes to an anterior

481   microdomain distinct from either VAP-1 or LIT-1 (Figure 6E-F). Further, as expected, VAP-1

482   localizes to an anterior microdomain distinct from AWC (Figure S7E-E'').

483

484   Since the KCC-3 and VAP-1 domains are mutually exclusive, we wondered if loss of either

485   microdomain affected the other. First, we examined if mutations in amphid channel-localized

486   proteins alter KCC-3 localization. We found that mutations in *daf-6, che-14,* and *lit-1,* but not *snx-*

487   *1,* affect KCC-3 localization, albeit only marginally (Figure 6G-H). In corollary, we also asked if

488   mutations in *kcc-3* reciprocally alter LIT-1 or VAP-1 expression. Again, we did not observe

489   obvious defects (Figure 6I-J'). Thus, while AMsh glial KCC-3 regulates the function of at least

490   the distal AWC neuron, the glia largely maintains its molecular microdomains between AFD and

491   channel neurons independently.

492

493   **KCC-3 localizes to apical micro-domains across multiple glia**

494   KCC-3 is broadly expressed in many *C. elegans* glia (Tanis, Bellemer, Moresco, Forbush, &

495   Koelle, 2009), but none of the other glia contact AWC or AFD-NRE. This led us to wonder if all

496   glia restrict KCC-3 localization similarly to AMsh. To test this, we examined KCC-3 localization

497   in two additional sheath glia: the polarized CEPsh at the anterior head of the animal and the PHsh

498   at the posterior tail of the animal. In both cells, KCC-3 localized to presumptive apical regions of

499   the glia, where it contacts cognate NREs (Figure 6K-L''). Thus, multiple glia localize the K/Cl

500   transporter KCC-3 to discrete apical domains, indicating that its restricted localization in glia likely

501   has broad functional relevance.

502

503   **DISCUSSION**

504   Using the discrete localization of glial KCC-3 around a single neuron-contact site (AFD-NRE) as

505   a facile molecular tool, we uncover that a single glial cell has an apical domain maintained by a

506 boundary zone (GAB). Further, it partitions its apical membrane into multiple and distinct

507 molecular microdomains around individual NRE-contact sites. Focusing on one microdomain cue,

508 the K/Cl transporter KCC-3, our genetic and structure-function studies reveal a two-step model for

509 KCC-3 localization. First, it localizes apically, and is then repelled by non-AFD ciliated NREs,

510 rendering it localized to the AFD-NRE (Figure 7). This mechanism is distinct from previously

511 reported regulators of K/Cl family transporters, and KCC-3 localization is required for it to

512 regulate AFD-NRE. Surprisingly, KCC-3 but not all glial microdomain cues, also impact distal

513 neurons. Thus, microdomain localization is important for the glia to compartmentalize cross-modal

514 sensory processing. Finally, we find that different glial microdomains are partially dependent on

515 each other. Thus, this exquisite sub-cellular organization within a glial cell may inform its ability

516 to integrate information across circuits.

517

518 **Glial apical membranes are molecularly asymmetric at individual neuron contact sites**

519 Our findings track prior studies to show that AMsh exhibit apical-basal polarity (Low et al., 2019).

520 Within even K/Cl co-transporters, we find those that localize either apically (KCC-3) or

521 basolaterally (KCC-1/2). Our studies further identify a 19 AA N-terminal sequence of KCC-2 as

522 necessary and sufficient to drive basolateral localization. In line with prior work on SAX-7, we

523 propose that basolateral targeting is the go/nogo gate that establishes apical-basal polarity for

524 AMsh glia. Sequence overlay does not detect any obvious basolateral-driving motifs shared

525 between SAX-7 and KCC-3, suggesting that multiple motifs may be at play.

526

527 The GAB zone boundary in AMsh glia overlays perfectly for all apically restricted molecules (PH-

528 PLCδ, KCC-3, SAX-7) and is not bound by tight junction proteins AJM-1 and DLG-1. This glial

529 cell-biology contrasts with that of epithelial apical-basal polarity and is conceptually analogous to

530 Axon Initial Segments (AIS) in neurons (Leterrier, 2018). We therefore propose that the AMsh

531 glial GAB is a sorting center like the neuronal AIS that delimits diffusion of membrane proteins

532 across different polarized cell domains, with impact on overlay of glia and NRE polarity. How this

533 zone develops or maintains will be interesting to dissect.

534

535 **Neuronal cilia signals regulate localization of glial regulatory cues**

536 Most mammalian cells have a primary, non-motile cilia. In neurons and glia, their presence and

537 functions are only recently being appreciated (Green & Mykytyn, 2014; Ki, Jeong, & Lee, 2021;

538 Sengupta, 2017). We find here that non-AFD ciliated NREs regulate localization of a glial

539 transporter at contacting glial membranes, through a signal transported by IFTA/B complex.

540 While further work is needed to identify the molecular identity of this cue, our data hint that this

541 may be independent of proximal extra-cellular vesicle release (Razzauti & Laurent, 2021) . To

542 our knowledge, while it has been demonstrated that glia track neuron activity (Agarwal et al.,

543 2017; Duan et al., 2020; Wang, D'Urso, & Bianchi, 2012; Yu et al., 2018), a role for neuronal

544 cilia in guiding glial properties and molecules has not yet been demonstrated.

545

546 **Glial microdomain localization of K/Cl transporters**

547 KCC-3 is a SLC12A6/K-Cl electroneutral transporter broadly implicated in neurological diseases

548 including autism, epilepsy, and schizophrenia (Boettger et al., 2003; Delpire & Kahle, 2017;

549 Garneau et al., 2017; Shekarabi et al., 2012). We previously showed that KCC-3 is a glial

550 regulator of neuron shape and functions (Singhvi et al., 2016). Here, we report that glial KCC-3

551 localizes to a microdomain around only AFD-NRE contact sites. Intriguingly, glia across species

552   localize KCC-3 to molecular microdomains. In rodents, Schwann cell peripheral glia localize

553   KCC-3 to apical microvilli around nodes (Sun, Lin, Tzeng, Delpire, & Shen, 2010). In mammals,

554   inner ear Deiter cells (glia-like support cells) localize KCC-3 to basal poles of hair cells

555   (Boettger et al., 2003; Ray & Singhvi, 2021). This is likely a specific regulation of KCC-3

556   proteins within glia, as we find that KCC-2 does not exhibit this localization when mis-expressed

557   in glia (Figure 3A-D). Further, this exquisitely specific localization is independent of the

558   canonical kinase regulators of K/Cl biology, WNK/SPAK/OSR kinases, which were identified

559   primarily in KCC-2 studies. Thus, how glia regulate KCC-3 is mechanistically distinct from how

560   other cell-types regulate KCC-1/2, underlining the importance of validating gene functions in

561   cell-specific contexts.

562

563   **Glial microdomains and cross-modal information processing**

564   We find that AMsh glia create distinct molecular microdomains of regulatory cues at different

565   neuron/NRE contact sites. AMsh glia also produce Ca^{2+} transients in response to different

566   sensory modalities. Thus, AMsh glia present a powerful experimental platform to overlay

567   molecular and functional microdomain activities with single glia-neuron resolution *in vivo*.

568

569   We also find that one microdomain-cue, KCC-3, can regulate sensory processing in distal NREs,

570   suggesting that its exquisite sub-cellular localization influences the glia's ability to

571   compartmentalize regulation of different contacting neurons. As this is not a general property of

572   all microdomain cues, and because we find that microdomains are largely regulated

573   independently, this raises the notion of specificity – how and why do glia regulate each cue

574   differently? And what does KCC-3's role in regulating both AWC and AFD imply for the

575   animal's ability to integrate information between these sensory modalities?

576

577   Finally, glia in both peripheral and central nervous systems interact with multiple neurons, and

578   mammalian astrocyte glia exhibit distinct microdomain patterns of intra-cellular Ca^{2+} transients

579   to different neuron activities (Agarwal et al., 2017; Khakh & Sofroniew, 2015). Whether

580   functional Ca^{2+} and molecular microdomains overlay causally awaits inquiry, but already leads

581   us to speculate that their overlay positions glia as integrators of information processing across

582   neural circuits.

583

596

597

598 **AUTHOR CONTRIBUTIONS**

599 SR and AS designed all studies, analyzed data and co-wrote the manuscript. SR performed all

600 experiments and was assisted by RSM and AK in construction of some strains and plasmids. PG

601 performed the functional Ca2+ imaging and analyzed the data with SR and AS.

602

603

604

605

606   **FIGURE LEGENDS**

607   **Figure 1. KCC-3 localizes to an apical region specifically around AFD-NRE**

608   **(A-A')** Schematic of a whole *C. elegans* (left) with boxed region zoomed in showing schematic

609   of AMsh glia (grey) and three contacting neurons (magenta, red, blue). (**B-B''**) Fluorescence

610   image merge (B) and single channel images of KCC-3 (green) labeled by a translational mScarlet

611   tag (B') and AMsh glia labeled by a cytosolic CFP (B''). Dotted boxed region is zoomed in C-I''.

612   Scale bar 10µm (**C-C''**). Fluorescent image merge (C) and single-channel images of KCC-3

613   (green) and AMsh glia (grey) showing restricted microdomain localization. Yellow arrow notes

614   one AMsh glial zone lacking KCC-3. (**D-D''**) Fluorescent image merge (D) and single-channel

615   images of KCC-3 (green, D') and AFD-NRE (magenta, D'') showing KCC-3 overlay on AFD-

616   NRE region, indicated by magenta asterisk. (**E-F**) Schematic of AMsh glial contact sites with

617   villi/AFD, channel, and embedded wing neurons as side profile (E) and top-down orthogonal view

618   (F). Only one of the bilateral glia-neuron pair is shown. Green, KCC-3 localization schematic. (**G-**

619   **I''**) Fluorescence images as merge (G, H, I) and single-channel images of KCC-3 (green, G', H',

620   I') and NRE of ASE (cyan, G''), AWA (red, H'') and AWC (red, I'') neurons. Non-overlap with

621   KCC-3 is denoted by white arrow, site of enrichment around AFD-NRE is noted by magenta

622   asterisk. Scale bar 5µm throughout unless otherwise noted.

623

624

625   **Figure 2: KCC-3 localizes to a glial apical microdomain in age-dependent manner.**

626   (**A**) Schematic of AMsh glia with apical and basolateral membranes marked. A= entire glia, A'=

627   zoom of boxed region in A around anterior ending. (**B-D**) Fluorescence image overlay (B-B'') of

628   glial membranes marked with apical (ApiGreen) and basolateral (BasoRed) domain markers. B'

629   = xz orthogonal projection, B''= yz orthogonal projection. Single-channel z-projection images of

630   BasoRed (C) and ApiGreen (D) in AMsh glia anterior endings. (**E-F''**) Fluorescence image

631   overlay (E, F) of tagged KCC-3 (green E', F') and apical membrane marker (magenta, E'', F'')

632   showing overlay with an apical microdomain. Yellow arrow denotes AMsh apical membrane

633   lacking KCC-3. White arrow in F-F'' denoted the GAB overlay seen in both apical marker and

634   KCC-3 tagged reporters. Magenta asterisk in E' and F' denotes region of enrichment around

635   AFD-NRE. (**G-G'**). Fluorescence image overlay (G) of tagged KCC-3 (green, G') with

636   basolateral membrane marker in AMsh (magenta, G''). Yellow arrow denotes region of non-

637   overlap. Magenta asterisk in H' denotes region of enrichment around AFD-NRE. (**H-H''**)

638   Fluorescence image overlay (H) of tagged KCC-3 (green, H') with tagged tight-junction protein,

639   AJM-1 (H''). Yellow arrow denotes AJM-1 staining around KCC-3 and AFD-NRE. White arrow

640   denotes the GAB of KCC-3 past AJM-1 staining. (**I-L**). Fluorescence images of tagged KCC-3,

641   expressed under P_{AMsh}-specific promoter, showing localization as early as L2/L3 larval animals,

642   and its aberrant expansion into non-AFD-NRE regions of the glia in aged Day10 adult animals

643   (yellow arrow). Magenta asterisk denotes region of enrichment around AFD-NRE. White arrow

644   denotes tail boundary. (**M**) Quantification of KCC-3 localization with age. N= number of

645   animals on graph. **** $p < 0.0001$, compared to Day 1 adults. Scale bar 5μm throughout unless

646   otherwise noted.

647

648 **Figure 3: Glial KCC-3 localization is regulated by distal non-AFD-NRE cilia**

649 **(A)** Quantification of KCC-3 localization in *tax-2, ttx-1,* and *gcy-8(ns355)* mutants compared to

650 WT. **(B)** Schematic of genetic and laser ablation protocols to assess KCC-3 localization without

651 AFD. **(C)** Quantification of KCC-3 localization in adults after genetic and laser ablation,

652 compared to mock animals. **(D)** Schematic showing that all amphid NREs contain cilia. **(E)**

653 KCC-3 localization in cilia mutants. **(F-F'')** Fluorescence image overlay (F) of tagged KCC-3

654 (F') and cytosolic glia marker (F'') of *dyf-19* cilia mutant animals. Scale bar, 5 μm **(G)**

655 Quantification of KCC-3 localization in amphid neuron identity mutants (*odr-7, ceh-37, ceh-36,*

656 *che-1*) and after wing neuron (AWA, AWB, AWC) laser ablation. **(H-I)** Quantification of KCC-

657 3 localization in DYF-11 rescue experiments (H). X refers to promoter(s) used for rescue

658 experiments. Identity of X and the neurons the promoter(s) express in are expanded on in I.

659 Orange denotes expression in associated neuron. ODR-4 expresses in an ASX and ADX neuron

660 but the exact identity of these neurons are unclear. This is denoted by the asterisk in these boxes.

661 For all graphs, * $p < 0.05$, ** $p < 0.01$, *** $p < 0.001$, **** $p < 0.0001$.

662

663 **Figure 4: Glial KCC-3 localizes in a two-step process through two protein regions**

664 **(A)** Phylogenetic tree denoting the relationship and sequence similarity of the three *C. elegans*

665 KCC proteins. **(B)** Quantification of KCC-1 and KCC-2 localization when expressed in AMsh

666 glia, compared to KCC-3. **(C-E)** Fluorescent images of KCC-1 (C), KCC-2 (D), and KCC-3 (E).

667 **(F)** Regions of high sequence dissimilarity between KCC-3 and KCC-1/2 from *in silico* sequence

668 alignment studies, with orange denoting regions of high sequence dissimilarity. **(G-I)**

669 Fluorescent images of KCC localization patterns seen in KCC chimeras. White arrow points to

670   apical expression beyond micro-domain. **(J)** Quantification of localization patterns chimeras

671   seen in KCC chimeras. **** p < 0.0001.

672

673   **Figure 5: Microdomain localization of KCC-3 regulates both AFD and non-AFD neuron**

674   **shape and associated animal behavior**

675   **(A-A')** Fluorescent images of AFD NRE in both wildtype (A) and *kcc-3(ok228)* mutants (A').

676   **(B)** Quantification of AFD NRE shape rescue with WT KCC-3, basolaterally localized KCC-

677   2/KCC-3 chimera, and an apically localized KCC-2/KCC-3 chimera. **(C-F')** Fluorescent images

678   of non-AFD amphid NRE shape in wildtype and *kcc-3(ok228)* mutant backgrounds. **(G)**

679   Schematic of chemotaxis assays, including equation for chemotaxis index (CI). **(H-J)** Behavioral

680   assay quantification for AWC-sensed odorants (H), AWA-sensed odorants (I) and ASE-sensed

681   tastant. All included at least 3 biological replicates with at least 90 animals/trial, except diacetyl,

682   which only had 2 biological replicates. All behavioral data compared to wildtype. * p < 0.05, **

683   p < 0.01, **** p < 0.0001.

684

685   **Figure 6: Micro-domains as a general feature of glia**

686   **(A-B)** Calcium transients evoked by addition of 0.01% isoamyl alcohol (IAA) in AWC neuron

687   expressing GCaMP6s upon single (A) or double (B) odor presentations. Solid lines represent the

688   average across 10 different animals in WT (blue) and *kcc-3* (red) background. Shaded areas

689   represent standard deviations. For double odor presentation, odor was presented at 10s and 50s

690   time-points, for 10s and 20s, respectively. N=10 animals **(C-D)** Peak calcium responses when

691   animal presented with 0.01% IAA (p = 0.043; Mann-Whitney) (C). Peak calcium responses

692   when IAA was removed (p = 0.0068; Mann-Whitney) (D). **(E-E'')** Fluorescence image overlay

693 (E) of KCC-3 (E') and VAP-1 (E''). **(F)** Schematic of VAP-1 and LIT-1 localization in AMsh

694 glia, with KCC-3. **(G)** Quantification of KCC-3 localization in *daf-6, che-14, and lit-1* mutants.

695 **(H)** Fluorescent image of KCC-3 in *lit-1* mutants. **(I-I')** Fluorescent images of VAP-1 in

696 wildtype (I) and *kcc-3* mutant (I') backgrounds. **(J-J')** Fluorescent image of LIT-1 in wildtype

697 (J) and *kcc-3* mutant (J') backgrounds. **(K-L'')** Fluorescent image overlay (K, L) of KCC-3 (K',

698 L') and cytosolic markers (K'', L'') in phasmid sheath glia (K-K'') and CEP sheath glia (L-L'').

699 *** p < 0.001. All scale bars at 5μm, except L-L'', which is at 10μm.

700

701 **Figure 7: Schematic of KCC-3 localization in AMsh glia**

702 KCC-3 localization is a two-step process. First, N-terminal sequences can guide KCC proteins to

703 basolateral membranes. Second, C-terminal sequences can determine apical vs. micro-domain

704 localization. Cilia also play a role in guiding KCC-3 from broad apical membranes to localized

705 micro-domain membranes.

706

707 **REFERENCES**

708 Agarwal, A., Wu, P. H., Hughes, E. G., Fukaya, M., Tischfield, M. A., Langseth, A. J., …

709 Bergles, D. E. (2017). Transient Opening of the Mitochondrial Permeability Transition Pore

710 Induces Microdomain Calcium Transients in Astrocyte Processes. *Neuron*, *93*(3), 587–

711 605.e7. https://doi.org/10.1016/j.neuron.2016.12.034

712 Albert, P. S., Brown, S. J., & Riddle, D. L. (1981). Sensory control of dauer larva formation in

713 Caenorhabditis elegans. *Journal of Comparative Neurology*, *198*(3), 435–451.

714 https://doi.org/10.1002/CNE.901980305

715 Alessi, D. R., Zhang, J., Khanna, A., Hochdörfer, T., Shang, Y., & Kahle, K. T. (2014). The

716 WNK-SPAK/OSR1 pathway: Master regulator of cation-chloride cotransporters. *Science*

717 *Signaling*, *7*(334), 1–11. https://doi.org/10.1126/scisignal.2005365

718 Allen, N. J., & Eroglu, C. (2017). Cell Biology of Astrocyte-Synapse Interactions. *Neuron*,

719 *96*(3), 697–708. https://doi.org/10.1016/j.neuron.2017.09.056

720 Bacaj, T., Lu, Y., & Shaham, S. (2008). The Conserved Proteins CHE-12 and DYF-11 Are

721 Required for Sensory Cilium Function in Caenorhabditis elegans. *Genetics*, *178*(2), 989.

722 https://doi.org/10.1534/GENETICS.107.082453

723 Bacaj, T., Tevlin, M., Lu, Y., & Shaham, S. (2009). Glia Are Essential for Sensory Organ

724 Function in C. elegans, *6*(5902), 247–253. https://doi.org/10.1111/j.1743-

725 6109.2008.01122.x.Endothelial

726 Bargmann, C. I., Hartwieg, E., & Horvitz, H. R. (1993). Odorant-selective genes and neurons

727 mediate olfaction in C. elegans. *Cell*, *74*(3), 515–527. https://doi.org/10.1016/0092-

728 8674(93)80053-H

729 Barres, B. A. (2008). Perspective The Mystery and Magic of Glia : A Perspective on Their Roles

730 in Health and Disease. *Neuron*, *60*(3), 430–440.

731 https://doi.org/10.1016/j.neuron.2008.10.013

732 Belin, S., Zuloaga, K. L., & Poitelon, Y. (2017). Influence of mechanical stimuli on schwann cell

733 biology. *Frontiers in Cellular Neuroscience*, *11*, 347.

734 https://doi.org/10.3389/FNCEL.2017.00347/BIBTEX

735 Blaesse, P., Airaksinen, M. S., Rivera, C., & Kaila, K. (2009). Cation-Chloride Cotransporters

736 and Neuronal Function. *Neuron*, *61*(6), 820–838.

737 https://doi.org/10.1016/j.neuron.2009.03.003

738 Boettger, T., Rust, M. B., Maier, H., Seidenbecher, T., Schweizer, M., Keating, D. J., … Jentsch,

739 T. J. (2003). Loss of K-Cl co-transporter KCC3 causes deafness, neurodegeneration and

740 reduced seizure threshold. *EMBO Journal*, *22*(20), 5422–5434.

741 https://doi.org/10.1093/emboj/cdg519

742 Burgess, A., Shah, K., Hough, O., & Hynynen, K. (2016). C. elegans S6K Mutants Require a

743 Creatine Kinase-Like Effector for Lifespan Extension, *15*(5), 477–491.

744 https://doi.org/10.1586/14737175.2015.1028369.Focused

745 Chalasani, S. H., Chronis, N., Tsunozaki, M., Gray, J. M., Ramot, D., Goodman, M. B., &

746 Bargmann, C. I. (2007). Dissecting a circuit for olfactory behaviour in Caenorhabditis

747 elegans. *Nature 2007 450:7166*, *450*(7166), 63–70. https://doi.org/10.1038/nature06292

748 Chung, W. S., Welsh, C. A., Barres, B. A., & Stevens, B. (2015). Do glia drive synaptic and

749 cognitive impairment in disease? *Nature Neuroscience*, *18*(11), 1539–1545.

750 https://doi.org/10.1038/nn.4142

751 Coburn, C. M., & Bargmann, C. I. (1996). A putative cyclic nucleotide-gated channel is required

752 for sensory development and function in C. elegans. *Neuron*, *17*(4), 695–706.

753   https://doi.org/10.1016/S0896-6273(00)80201-9

754   Delpire, E., & Kahle, K. T. (2017). The KCC3 cotransporter as a therapeutic target for peripheral

755   neuropathy. *Expert Opinion on Therapeutic Targets*, *21*(2), 113–116.

756   https://doi.org/10.1080/14728222.2017.1275569

757   Ding, G., Zou, W., Zhang, H., Xue, Y., Cai, Y., Huang, G., … Kang, L. (2015). In Vivo tactile

758   stimulation-evoked responses in Caenorhabditis elegans amphid sheath glia. *PLoS ONE*,

759   *10*(2). https://doi.org/10.1371/journal.pone.0117114

760   Duan, D., Zhang, H., Yue, X., Fan, Y., Xue, Y., Shao, J., … Kang, L. (2020). Sensory Glia

761   Detect Repulsive Odorants and Drive Olfactory Adaptation. *Neuron*, *108*(4), 707–721.e8.

762   https://doi.org/10.1016/j.neuron.2020.08.026

763   Dwyer, N. D., Adler, C. E., Crump, J. G., L'Etoile, N. D., & Bargmann, C. I. (2001). Polarized

764   Dendritic Transport and the AP-1 µ1 Clathrin Adaptor UNC-101 Localize Odorant

765   Receptors to Olfactory Cilia. *Neuron*, *31*(2), 277–287. https://doi.org/10.1016/S0896-

766   6273(01)00361-0

767   Eroglu, Ç., Allen, N. J., Susman, M. W., O'Rourke, N. A., Park, C. Y., Özkan, E., … Barres, B.

768   A. (2009). Gabapentin Receptor α2δ-1 Is a Neuronal Thrombospondin Receptor

769   Responsible for Excitatory CNS Synaptogenesis. *Cell*, *139*(2), 380–392.

770   https://doi.org/10.1016/j.cell.2009.09.025

771   Gallemore, R. P., Hughes, B. A., & Miller, S. S. (1997). Retinal pigment epithelial transport

772   mechanisms and their contributions to the electroretinogram. *Progress in Retinal and Eye*

773   *Research*, *16*(4), 509–566. https://doi.org/10.1016/S1350-9462(96)00037-7

774   Garneau, A. P., Marcoux, A.-A., Frenette-Cotton, R., Mac-Way, F., Lavoie, J. L., & Isenring, P.

775   (2017). Molecular insights into the normal operation, regulation and multisystemic roles of

776   K^+-Cl^- cotransporter 3 (KCC3). *American Journal of Physiology - Cell Physiology*, *3*,

777   ajpcell.00106.2017. https://doi.org/10.1152/ajpcell.00106.2017

778 Goodman, M. B., & Sengupta, P. (2018). The extraordinary AFD thermosensor of C. elegans.

779   *Pflugers Archiv : European Journal of Physiology*, *470*(5), 839.

780   https://doi.org/10.1007/S00424-017-2089-5

781 Green, J. A., & Mykytyn, K. (2014). Neuronal Primary Cilia: An Underappreciated Signaling

782   and Sensory Organelle in the Brain. *Neuropsychopharmacology*, *39*(1), 244.

783   https://doi.org/10.1038/NPP.2013.203

784 Hisamoto, N., Moriguchi, T., Urushiyama, S., Mitani, S., Shibuya, H., & Matsumoto, K. (2008).

785   Caenorhabditis elegans WNK-STE20 pathway regulates tube formation by modulating ClC

786   channel activity. *EMBO Reports*, *9*(1), 70–75. https://doi.org/10.1038/sj.embor.7401128

787 Howell, K., & Hobert, O. (2017). Morphological Diversity of C. elegans Sensory Cilia Instructed

788   by the Differential Expression of an Immunoglobulin Domain Protein. *Current Biology :*

789   *CB*, *27*(12), 1782–1790.e5. https://doi.org/10.1016/J.CUB.2017.05.006

790 Huang, T. T., Matsuyama, H. J., Tsukada, Y., Singhvi, A., Syu, R. T., Lu, Y., … Pan, C. L.

791   (2020). Age-dependent changes in response property and morphology of a thermosensory

792   neuron and thermotaxis behavior in Caenorhabditis elegans. *Aging Cell*, *19*(5).

793   https://doi.org/10.1111/ACEL.13146

794 Inada, H., Ito, H., Satterlee, J., Sengupta, P., Matsumoto, K., & Mori, I. (2006). Identification of

795   Guanylyl Cyclases That Function in Thermosensory Neurons of Caenorhabditis elegans.

796   *Genetics*, *172*(4), 2239–2252. https://doi.org/10.1534/GENETICS.105.050013

797 Kaila, K., Price, T. J., Payne, J. A., Puskarjov, M., & Voipio, J. (2014). Cation-chloride

798   cotransporters in neuronal development, plasticity and disease. *Nature Reviews*

799   *Neuroscience*, *15*(10), 637–654. https://doi.org/10.1038/nrn3819

800   Khakh, B. S., & Sofroniew, M. V. (2015). Diversity of astrocyte functions and phenotypes in

801   neural circuits. *Nature Neuroscience*, *18*(7), 942–952. https://doi.org/10.1038/nn.4043

802   Ki, S. M., Jeong, H. S., & Lee, J. E. (2021). Primary Cilia in Glial Cells: An Oasis in the Journey

803   to Overcoming Neurodegenerative Diseases. *Frontiers in Neuroscience*, *15*, 1227.

804   https://doi.org/10.3389/FNINS.2021.736888/BIBTEX

805   Kimura, K. D., Miyawaki, A., Matsumoto, K., & Mori, I. (2004). The C. elegans Thermosensory

806   Neuron AFD Responds to Warming. *Current Biology*, *14*(14), 1291–1295.

807   https://doi.org/10.1016/J.CUB.2004.06.060

808   Lanjuin, A., VanHoven, M. K., Bargmann, C. I., Thompson, J. K., & Sengupta, P. (2003).

809   Otx/otd homeobox genes specify distinct sensory neuron identities in C. elegans.

810   *Developmental Cell*, *5*(4), 621–633. https://doi.org/10.1016/s1534-5807(03)00293-4

811   Lechtreck, K. F. (2015). IFT-cargo interactions and protein transport in cilia. *Trends in*

812   *Biochemical Sciences*, *40*(12), 765. https://doi.org/10.1016/J.TIBS.2015.09.003

813   Leterrier, C. (2018). The Axon Initial Segment: An Updated Viewpoint. *Journal of*

814   *Neuroscience*, *38*(9), 2135–2145. https://doi.org/10.1523/JNEUROSCI.1922-17.2018

815   Low, I. I. C., Williams, C. R., Chong, M. K., Mclachlan, I. G., Wierbowski, B. M., Kolotuev, I.,

816   & Heiman, M. G. (2019). Morphogenesis of neurons and glia within an epithelium.

817   https://doi.org/10.1242/dev.171124

818   Mahon, M. J. (2011). Apical membrane segregation of phosphatidylinositol-4,5-bisphosphate

819   influences parathyroid hormone 1 receptor compartmental signaling and localization via

820   direct regulation of ezrin in LLC-PK1 cells. *Cellular Signalling*, *23*(10), 1659.

821   https://doi.org/10.1016/J.CELLSIG.2011.05.020

822   Martin, C. G., Bent, J. S., & Singhvi, A. (2022). Epithelia delimits glial apical polarity against

823   mechanical shear to maintain glia-neuron - architecture. *BioRxiv*, 2022.12.26.521704.

824   https://doi.org/10.1101/2022.12.26.521704

825   McMahon, L., Legouis, R., Vonesch, J. L., & Labouesse, M. (2001). Assembly of C. elegans

826   apical junctions involves positioning and compaction by LET-413 and protein aggregation

827   by the MAGUK protein DLG-1. *Journal of Cell Science*, *114*(12), 2265–2277.

828   https://doi.org/10.1242/JCS.114.12.2265

829   Nehme, R., & Conradt, B. (2009). egl-1: a key activator of apoptotic cell death in C. elegans.

830   *Oncogene 2009 27:1*, *27*(1), S30–S40. https://doi.org/10.1038/onc.2009.41

831   Oikonomou, G., Perens, E. A., Lu, Y., Watanabe, S., Jorgensen, E. M., & Shaham, S. (2011).

832   Opposing Activities of LIT-1/NLK and DAF-6/Patched-Related Direct Sensory

833   Compartment Morphogenesis in C. elegans. *PLoS Biology*, *9*(8), e1001121.

834   https://doi.org/10.1371/journal.pbio.1001121

835   Oikonomou, G., & Shaham, S. (2011). The glia of caenorhabditis elegans. *Glia*, *59*(9), 1253–

836   1263. https://doi.org/10.1002/glia.21084

837   Payne, J. A., Rivera, C., Voipio, J., & Kaila, K. (2003). Cation-chloride co-transporters in

838   neuronal communication, development and trauma. *Trends in Neurosciences*, *26*(4), 199–

839   206. https://doi.org/10.1016/S0166-2236(03)00068-7

840   Perens, E. A., & Shaham, S. (2005). C. elegans daf-6 encodes a patched-related protein required

841   for lumen formation. *Developmental Cell*, *8*(6), 893–906.

842   https://doi.org/10.1016/j.devcel.2005.03.009

843   Perkins, L. A., Hedgecock, E. M., Thomson, J. N., & Culotti, J. G. (1986). Mutant sensory cilia

844   in the nematode Caenorhabditis elegans. *Developmental Biology*, *117*(2), 456–487.

845   https://doi.org/10.1016/0012-1606(86)90314-3

846   Pogodalla, N., Kranenburg, H., Rey, S., Rodrigues, S., Cardona, A., & Klämbt, C. (2021).

847   Drosophila ßHeavy-Spectrin is required in polarized ensheathing glia that form a diffusion-

848   barrier around the neuropil. *Nature Communications*, *12*(1).

849   https://doi.org/10.1038/S41467-021-26462-X

850   Raiders, S., Han, T., Scott-Hewitt, N., Kucenas, S., Lew, D., Logan, M. A., & Singhvi, A.

851   (2021). Engulfed by Glia: Glial Pruning in Development, Function, and Injury across

852   Species. *The Journal of Neuroscience*, JN-SY-1660-20.

853   https://doi.org/10.1523/JNEUROSCI.1660-20.2020

854   Ray, S., & Singhvi, A. (2021). Charging Up the Periphery: Glial Ionic Regulation in Sensory

855   Perception. *Frontiers in Cell and Developmental Biology*, *9*, 1989.

856   https://doi.org/10.3389/FCELL.2021.687732/BIBTEX

857   Razzauti, A., & Laurent, P. (2021). Ectocytosis prevents accumulation of ciliary cargo in c.

858   Elegans sensory neurons. *ELife*, *10*. https://doi.org/10.7554/ELIFE.67670

859   Salin-Cantegrel, A., Rivière, J. B., Shekarabi, M., Rasheed, S., DaCal, S., Laganière, J., …

860   Rouleau, G. A. (2011). Transit defect of potassium-chloride co-transporter 3 is a major

861   pathogenic mechanism in hereditary motor and sensory neuropathy with agenesis of the

862   corpus callosum. *Journal of Biological Chemistry*, *286*(32), 28456–28465.

863   https://doi.org/10.1074/jbc.M111.226894

864   Satterlee, J. S., Sasakura, H., Kuhara, A., Berkeley, M., Mori, I., & Sengupta, P. (2001).

865   Specification of thermosensory neuron fate in C. elegans requires ttx-1, a homolog of

866   otd/Otx. *Neuron*, *31*(6), 943–956. https://doi.org/10.1016/S0896-6273(01)00431-7

867   Sengupta, P. (2017). Cilia and sensory signaling: The journey from "animalcules" to human

868   disease. *PLOS Biology*, *15*(4), e2002240.

869   https://doi.org/10.1371/JOURNAL.PBIO.2002240

870   Sengupta, P., Colbert, H. A., & Bargmann, C. I. (1994). The C. elegans gene odr-7 encodes an

871   olfactory-specific member of the nuclear receptor superfamily. *Cell*, *79*(6), 971–980.

872   https://doi.org/10.1016/0092-8674(94)90028-0

873   Shekarabi, M., Moldrich, R. X., Rasheed, S., Salin-Cantegrel, A., Laganiere, J., Rochefort, D.,

874   … Rouleau, G. A. (2012). Loss of Neuronal Potassium/Chloride Cotransporter 3 (KCC3) Is

875   Responsible for the Degenerative Phenotype in a Conditional Mouse Model of Hereditary

876   Motor and Sensory Neuropathy Associated with Agenesis of the Corpus Callosum. *Journal

877   of Neuroscience*, *32*(11), 3865–3876. https://doi.org/10.1523/JNEUROSCI.3679-11.2012

878   Shin, K., Fogg, V. C., & Margolis, B. (2006). Tight Junctions and Cell Polarity.

879   *Https://Doi.Org/10.1146/Annurev.Cellbio.22.010305.104219*, *22*, 207–235.

880   https://doi.org/10.1146/ANNUREV.CELLBIO.22.010305.104219

881   Simard, C. F., Bergeron, M. J., Frenette-Cotton, R., Carpentier, G. A., Pelchat, M. E., Caron, L.,

882   & Isenring, P. (2007). Homooligomeric and Heterooligomeric Associations between K+-

883   Cl– Cotransporter Isoforms and between K+-Cl– and Na+-K+-Cl– Cotransporters. *Journal

884   of Biological Chemistry*, *282*(25), 18083–18093. https://doi.org/10.1074/JBC.M607811200

885   Singhvi, A., Liu, B., Friedman, C. J., Fong, J., Lu, Y., Huang, X. Y., & Shaham, S. (2016). A

886   Glial K/Cl Transporter Controls Neuronal Receptive Ending Shape by Chloride Inhibition

887   of an rGC. *Cell*, *165*(4), 936–948. https://doi.org/10.1016/j.cell.2016.03.026

888   Singhvi, A., & Shaham, S. (2019). Glia-Neuron Interactions in *Caenorhabditis elegans*. *Annual

889   Review of Neuroscience*, *42*(1), 149–168. https://doi.org/10.1146/annurev-neuro-070918-

890   050314

891   Singhvi, A., Shaham, S., & Rapti, G. (2023). Glia development and function in the nervous

892   system of Caenorhabditis elegans. *Cold Spring Harbor Perspectives in Biology*, *(in press)*.

893   Sparrow, J. R., Hicks, D., & Hamel, C. P. (2010). The Retinal Pigment Epithelium in Health and

894   Disease. *Current Molecular Medicine*, *10*(9), 802–823.

895   https://doi.org/10.2174/156652410793937813

896   Stogsdill, J. A., Ramirez, J., Liu, D., Kim, Y. H., Baldwin, K. T., Enustun, E., … Eroglu, C.

897   (2017). Astrocytic neuroligins control astrocyte morphogenesis and synaptogenesis. *Nature*,

898   *551*(7679), 192–197. https://doi.org/10.1038/nature24638

899   Strauss, O. (2005). The Retinal Pigment Epithelium in Visual Function. *Physiological Reviews*,

900   *85*, 845–881. https://doi.org/10.1152/physrev.00021.2004.

901   Sulston, J. E. (1983). Neuronal cell lineages in the nematode Caenorhabditis elegans. *Cold

902   Spring Harbor Symposia on Quantitative Biology*, *48 Pt 2*, 443–452.

903   https://doi.org/10.1101/sqb.1983.048.01.049

904   Sun, Y. T., Lin, T. S., Tzeng, S. F., Delpire, E., & Shen, M. R. (2010). Deficiency of

905   electroneutral K+-Cl- cotransporter 3 causes a disruption in impulse propagation along

906   peripheral nerves. *Glia*, *58*(13), 1544–1552. https://doi.org/10.1002/glia.21028

907   Swoboda, P., Adler, H. T., & Thomas, J. H. (2000). The RFX-type transcription factor DAF-19

908   regulates sensory neuron cilium formation in C. elegans. *Molecular Cell*, *5*(3), 411–421.

909   https://doi.org/10.1016/S1097-2765(00)80436-0

910   Tanis, J. E., Bellemer, A., Moresco, J. J., Forbush, B., & Koelle, M. R. (2009). The Potassium

911   Chloride Cotransporter KCC-2 Coordinates Development of Inhibitory Neurotransmission

912   and Synapse Structure in Caenorhabditis elegans. *Journal of Neuroscience*, *29*(32), 9943–

913   9954. https://doi.org/10.1523/JNEUROSCI.1989-09.2009

914 Uchida, O., Nakano, H., Koga, M., & Ohshima, Y. (2003, April). The C. elegans che-1 gene

915 encodes a zinc finger transcription factor required for specification of the ASE

916 chemosensory neurons. *Development*. Development. https://doi.org/10.1242/dev.00341

917 von Bartheld, C. S., Bahney, J., & Herculano-Houzel, S. (2016). The Search for True Numbers

918 of Neurons and Glial Cells in the Human Brain: A Review of 150 Years of Cell Counting.

919 *The Journal of Comparative Neurology*, *524*(18), 3865. https://doi.org/10.1002/CNE.24040

920 Wallace, S. W., Singhvi, A., Liang, Y., Lu, Y., Shaham, S., Wallace, S. W., … Shaham, S.

921 (2016). PROS-1 / Prospero Is a Major Regulator of the Glia- Specific Secretome

922 Controlling Sensory-Neuron Shape and Function in C . elegans Article PROS-1 / Prospero

923 Is a Major Regulator of the Glia-Specific Secretome Controlling Sensory-Neuron Shape and

924 Function. *CellReports*, *15*(3), 550–562. https://doi.org/10.1016/j.celrep.2016.03.051

925 Wang, Y., D'Urso, G., & Bianchi, L. (2012). Knockout of glial channel ACD-1 exacerbates

926 sensory deficits in a C. elegans mutant by regulating calcium levels of sensory neurons.

927 *Journal of Neurophysiology*, *107*(1), 148–158. https://doi.org/10.1152/jn.00299.2011

928 White, J. G., Southgate, E. ., Thomson, J. . N. ., & Brenner, S. . (2008). The Structure of the

929 Nervous System of the Nematode Caenorhabditis elegans, *314*(1165), 1–340.

930 Yoshida, A., Nakano, S., Suzuki, T., Ihara, K., Higashiyama, T., & Mori, I. (2016). A glial

931 K+/Cl-cotransporter modifies temperature-evoked dynamics in Caenorhabditis elegans

932 sensory neurons. *Genes, Brain and Behavior*, *15*(4), 429–440.

933 https://doi.org/10.1111/gbb.12260

934 Yu, X., Taylor, A. M. W., Nagai, J., Golshani, P., Evans, C. J., Coppola, G., & Khakh, B. S.

935 (2018). Reducing Astrocyte Calcium Signaling In Vivo Alters Striatal Microcircuits and

936 Causes Repetitive Behavior. *Neuron*, *99*(6), 1170–1187.e9.

937   https://doi.org/10.1016/j.neuron.2018.08.015

938

Figure 1 Ray et al

Figure 2

Figure 3

Figure 4

Figure 4

Figure 5   Ray et al

$$CI = \frac{A - B}{A + B}$$

Figure 6   Ray et al
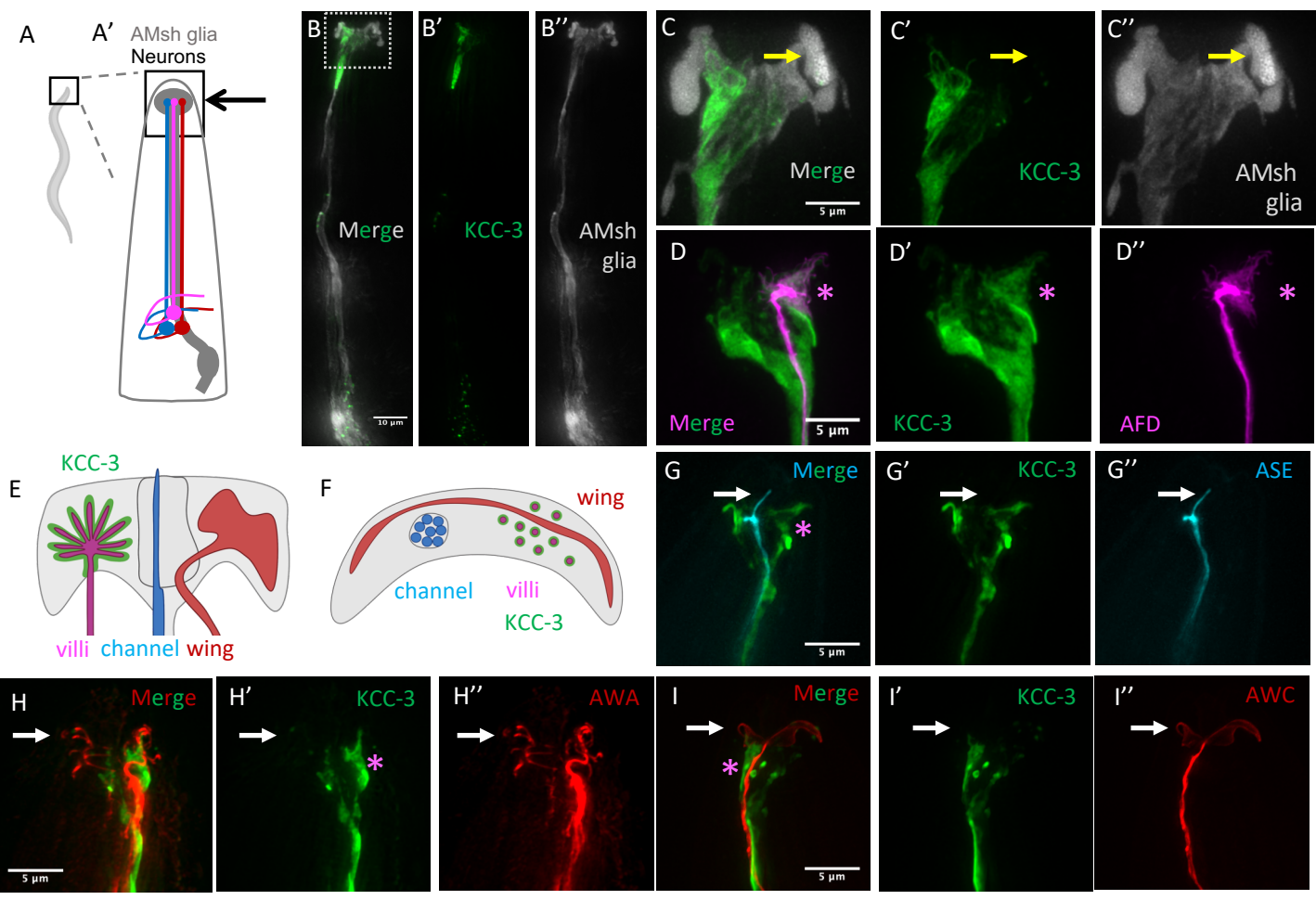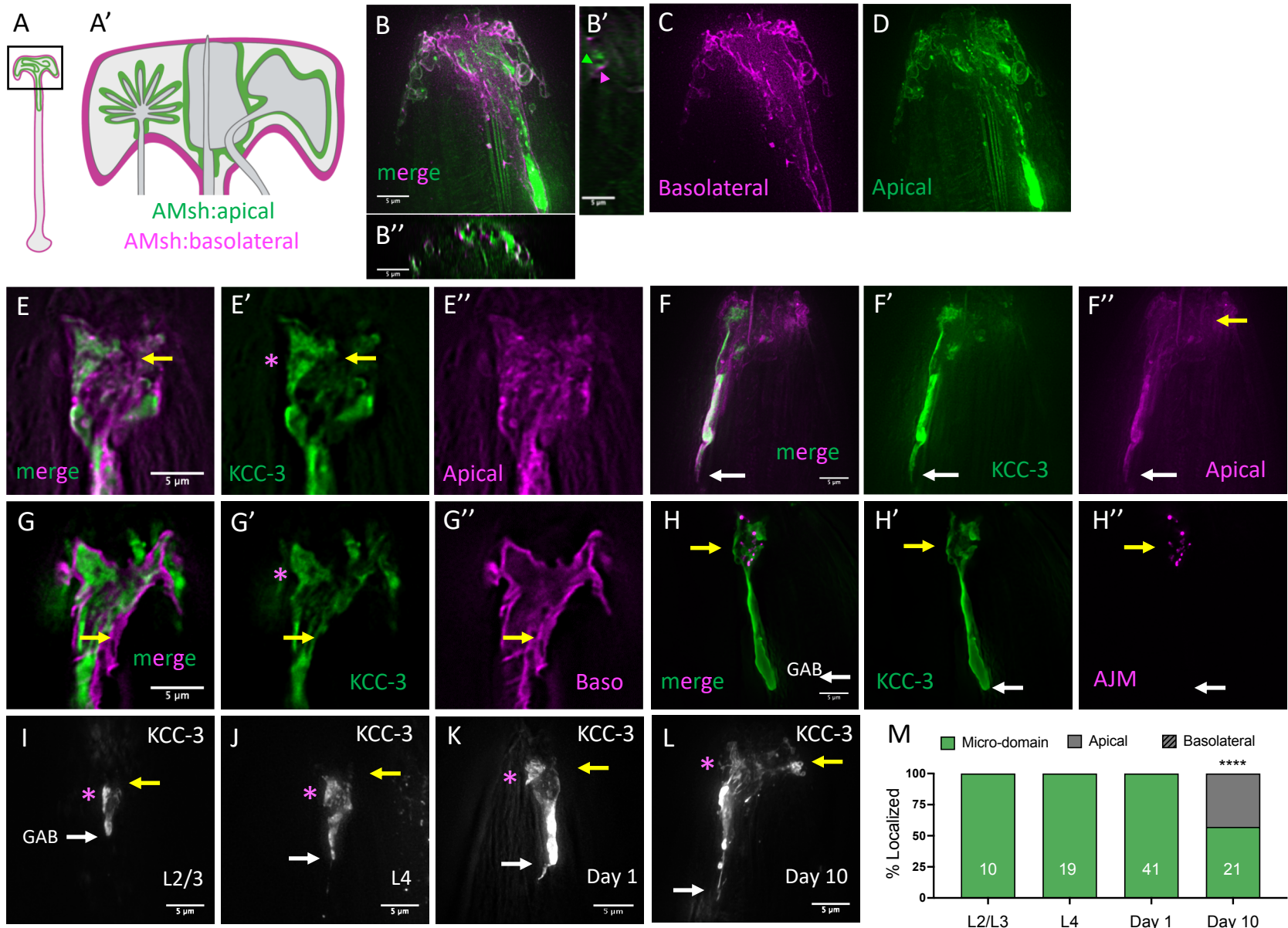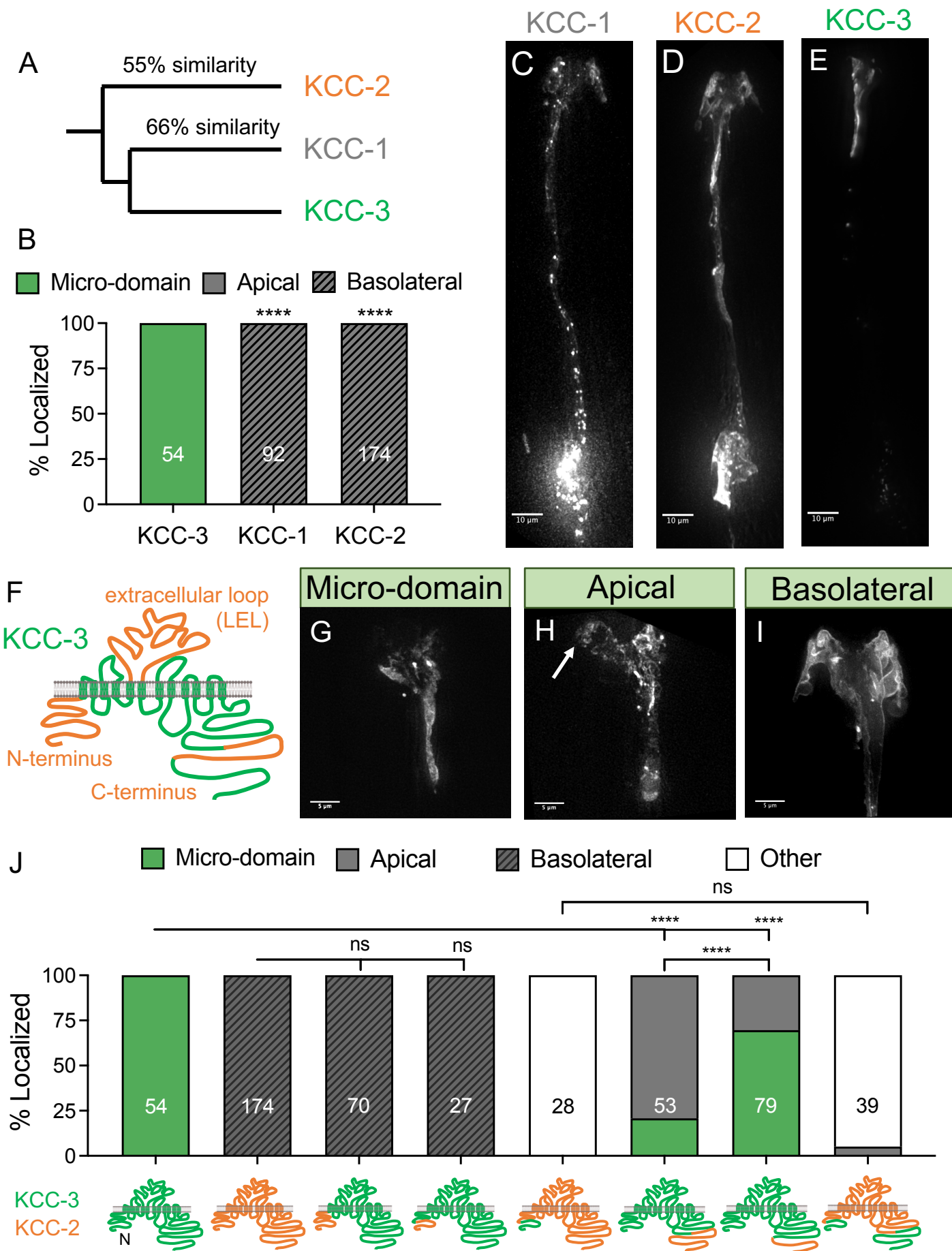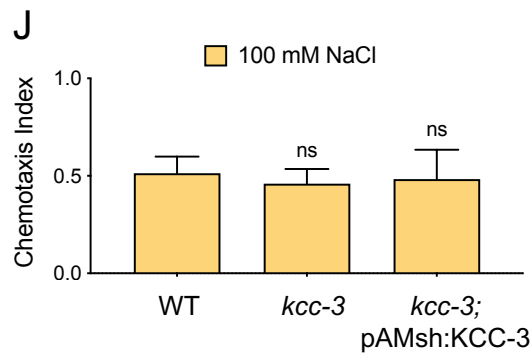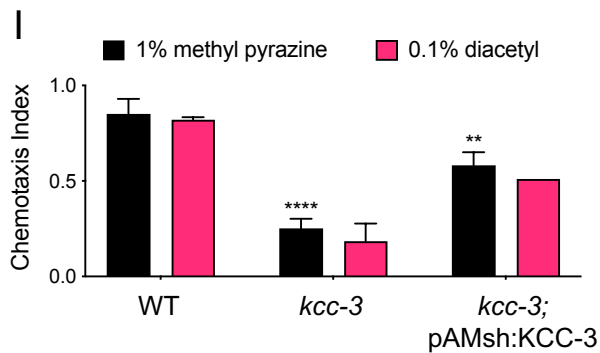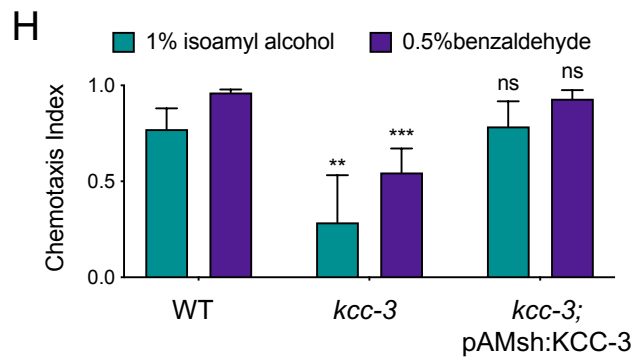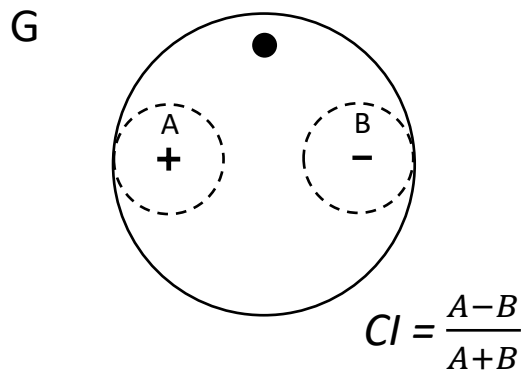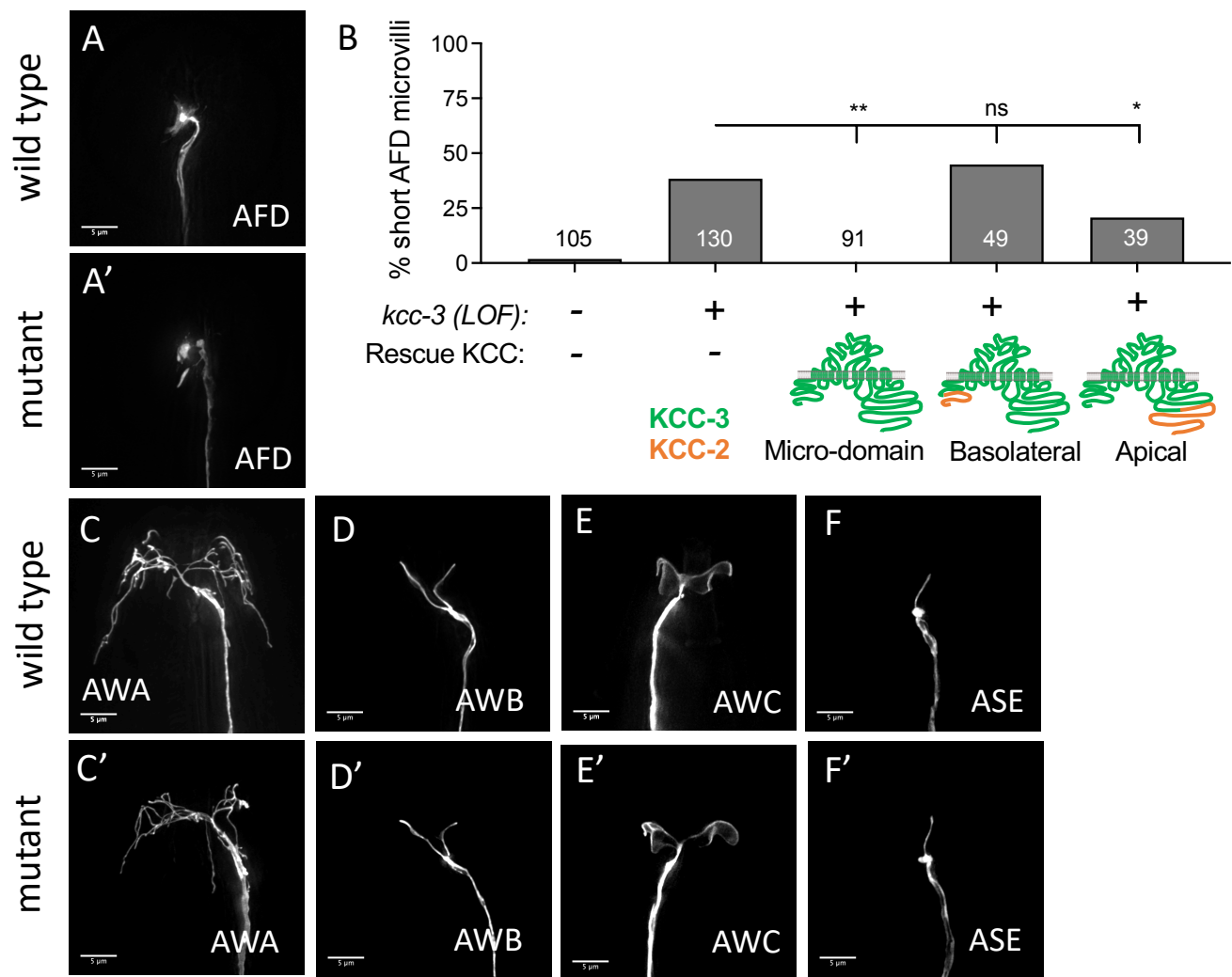
Figure 7
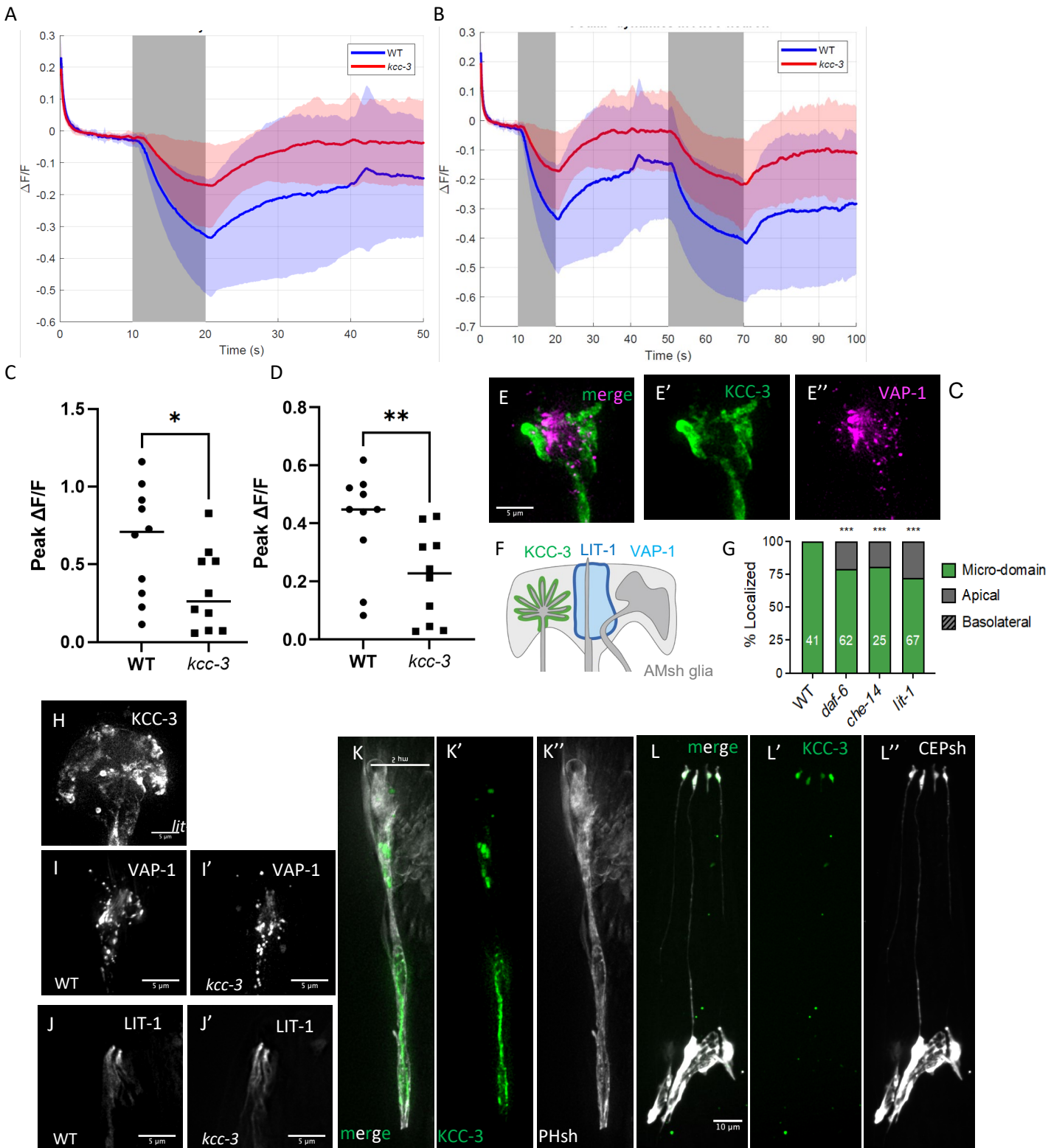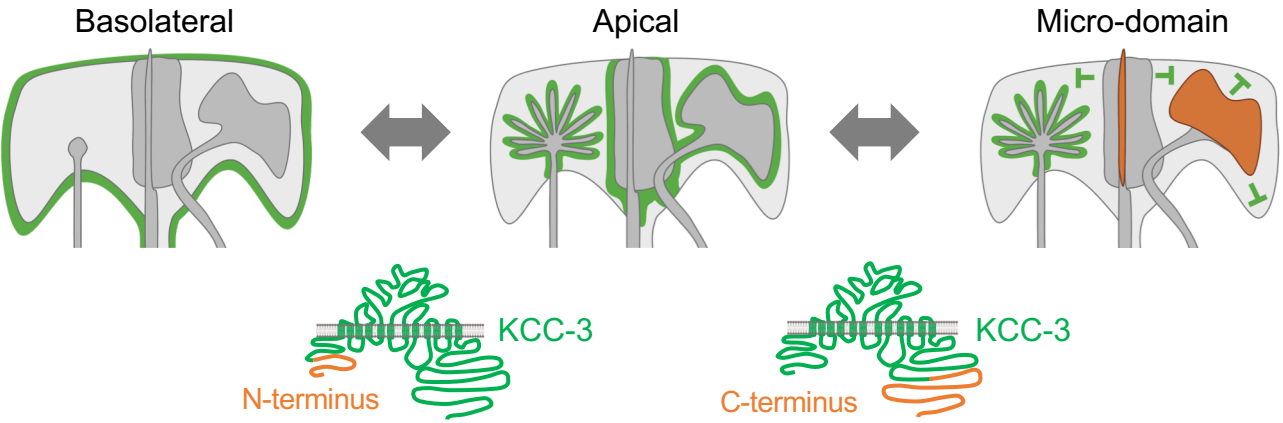
- N-terminal intracellular sequences
- C-terminal intracellular sequences
- Non-cell autonomous
- Cilia proteins (membrane or secreted?)